2013

Genomics of a Metamorphic Timing QTL: Met1 Maps to a Unique Genomic Position and Regulates Morph and Species-Specific Patterns of Brain Transcription

Robert B. Page
University of Louisville

Meredith A. Boley
University of Kentucky, mboley@gmail.com

David K. Kump
University of Kentucky, kevinkump@uky.edu

Stephen R. Voss
University of Kentucky, srvoss@uky.edu

Genomics of a Metamorphic Timing QTL: Met1 Maps to a Unique Genomic Position and Regulates Morph and Species-Specific Patterns of Brain Transcription

Notes/Citation Information
Published in *Genome Biology and Evolution*, v. 5, no. 9, p. 1716-1730.

Digital Object Identifier (DOI)
http://dx.doi.org/10.1093/gbe/evt123

Genomics of a Metamorphic Timing QTL: *met1* Maps to a Unique Genomic Position and Regulates Morph and Species-Specific Patterns of Brain Transcription

Robert B. Page[1,3,*], Meredith A. Boley[2], David K. Kump[2], and Stephen R. Voss[2,*]

[1]Department of Biology, University of Louisville

[2]Department of Biology & Spinal Cord and Brain Injury Research Center, University of Kentucky

[3]Present address: Department of Biology, College of St. Benedict & St. John's University, Collegeville, MN

*Corresponding author: E-mail: rbp0554@gmail.com; srvoss@uky.edu.

Accepted: August 9, 2013

Abstract

Very little is known about genetic factors that regulate life history transitions during ontogeny. Closely related tiger salamanders (*Ambystoma* species complex) show extreme variation in metamorphic timing, with some species foregoing metamorphosis altogether, an adaptive trait called paedomorphosis. Previous studies identified a major effect quantitative trait locus (*met1*) for metamorphic timing and expression of paedomorphosis in hybrid crosses between the biphasic Eastern tiger salamander (*Ambystoma tigrinum tigrinum*) and the paedomorphic Mexican axolotl (*Ambystoma mexicanum*). We used existing hybrid mapping panels and a newly created hybrid cross to map the *met1* genomic region and determine the effect of *met1* on larval growth, metamorphic timing, and gene expression in the brain. We show that *met1* maps to the position of a urodele-specific chromosome rearrangement on linkage group 2 that uniquely brought functionally associated genes into linkage. Furthermore, we found that more than 200 genes were differentially expressed during larval development as a function of *met1* genotype. This list of differentially expressed genes is enriched for proteins that function in the mitochondria, providing evidence of a link between *met1*, thyroid hormone signaling, and mitochondrial energetics associated with metamorphosis. Finally, we found that *met1* significantly affected metamorphic timing in hybrids, but not early larval growth rate. Collectively, our results show that *met1* regulates species and morph-specific patterns of brain transcription and life history variation.

Key words: amphibian, comparative genomics, linkage mapping, microarray, metamorphic timing, QTL.

Introduction

Some closely related species exhibit dramatic phenotypic differences of adaptive significance. Such species provide excellent models to investigate the genetic basis of complex traits and life history evolution. An important and difficult objective in working with natural species is to identify gene and gene functions that are associated with phenotypic differences (Jones 1998; Bradshaw and Schemske 2003; Hoekstra et al. 2006). In some cases, potential candidate genes are predictable given the nature of the phenotypic differences, such as in the case of color polymorphisms (Mundy 2007) and craniofacial variations in birds and fishes (Schneider and Helms 2003; Streelman et al. 2007). However, for most traits, it is difficult to predict genetic and developmental components of the selection process. When it is possible to cross species and segregate molecular and phenotypic variation, quantitative trait locus (QTL) mapping provides an unbiased and efficient method to initially locate genetic factors in the genome. Subsequent comparative and functional genomic approaches can then be used to narrow the search for causative genetic factors and reveal insights about gene functions, development, and evolution.

Here, we consider genetic factors that activate postembryonic developmental programs during ontogeny to enable critical life history transitions. Amphibian and insect larvae undergo a dramatic life history transition known as metamorphosis, during which adult traits develop to enable strategies for predator avoidance, dispersal, resource utilization, and mating (Wilbur 1980). Thyroid hormone (TH) is the master regulator of amphibian metamorphosis, and release of TH by the thyroid is under complex control of the hypothalamic–pituitary–thyroid axis (Shi 2000; Denver et al. 2002).

At a molecular level, the effects of TH are mediated by TH receptors, which are nuclear transcription factors that regulate the transcription of genes in a TH-dependent manner (Buchholz et al. 2006). Thus, rising TH levels during larval development bring about metamorphosis by triggering transcriptional programs that activate tissue remodeling, cellular differentiation, and tissue regression—developmental processes that transform larval phenotypes into adult phenotypes (Shi 2000). According to this model, variation in metamorphic timing may trace to variation in the timing of TH-dependent transcriptional events during development.

The timing of metamorphosis is a critical life history trait that evolves in response to aquatic habitat characteristics that determine the rate and plasticity of larval growth and the length of the larval period (Wilbur and Collins 1973; Wilbur 1980; Semlitsch and Wilbur 1989). Species that use relatively permanent habitats for larval development generally have longer larval periods than species that use ephemeral habitats. For example, some anuran tadpoles hatch in rapidly drying desert ponds and metamorphose after only 8 days of development (Newman 1989), whereas salamanders in permanent, high altitude lakes may overwinter as aquatic larvae and transform the following year, or forgo metamorphosis altogether (Petranka 1998). The observation of life history variation between anuran and salamander species is not surprising because these groups diverged from a common ancestor more than 300 Ma. However, there are also substantial differences in developmental timing within both of these orders, of which the pronounced differences in metamorphic timing between closely related tiger salamander lineages (*Ambystoma* spp.) are an unusually dramatic example. Such species groups provide models for identifying genes for metamorphic timing and investigating the relationships between development, life history variation, and life cycle evolution (Voss et al. 2003, 2012; Voss and Smith 2005).

In most Eastern tiger salamander (*A. tigrinum tigrinum*) populations, larvae undergo an obligate metamorphosis after a variable period of growth (Petranka 1998). In contrast, Mexican axolotls (*A. mexicanum*) do not produce a high titer of TH during larval development and thus do not metamorphose (Prahlad 1968; Galton 1992), a process called paedomorphosis (Gould 1977). As a consequence, sexually mature *A. mexicanum* retain juvenile traits and complete their life cycles in the aquatic habitat. Crosses between *A. t. tigrinum* and *A. mexicanum*, followed by backcrosses of F1 hybrids to *A. mexicanum*, show that a major effect QTL (*met1*) explains both continuous variation in metamorphic timing and expression of paedomorphosis (Voss and Shaffer 1997, 2000; Voss and Smith 2005; Voss et al. 2012). Heterozygotes that inherit a single *A. t. tigrinum met1* allele almost invariably undergo metamorphosis. However, homozygotes that inherit two *A. mexicanum met1* alleles metamorphose at a later time than heterozygotes, or fail to undergo metamorphosis altogether and exhibit paedomorphosis. The number of paedomorphs observed from hybrid crosses depends on genetic background. For example, when hybrid crosses are made using *A. mexicanum* from a laboratory population, the observed number of paedomorphs is statistically consistent with a single gene model (Voss 1995). However, when hybrid crosses are made using wild-caught *A. mexicanum*, a more complicated genetic basis is implicated and fewer paedomorphs are observed than expected under a single gene model. In these crosses, most of the *A. mexicanum met1* homozygotes do not exhibit paedomorphosis. Instead, they metamorphose on average 36 days later than siblings carrying an *A. t. tigrinum met1* allele (Voss and Shaffer 1997, 2000; Voss and Smith 2005). Thus, *met1* alleles from paedomorphic *A. mexicanum* delay metamorphosis while *met1* alleles from metamorphic *A. t. tigrinum* decrease the time to metamorphosis, and this consequently decreases the probability of expressing paedomorphosis.

In this study, we used comparative, quantitative, and functional genomic approaches to map the *met1* genomic region and investigate the effect of *met1* genotype on larval growth, neurodevelopmental gene expression, and metamorphic timing. Our previous work identified *met1* using anonymous molecular markers (Voss and Shaffer 1997, 2000). Subsequently, an expressed sequence tag (EST) (*ctg325*) was identified for *met1* that shows nucleotide similarity to human *ngfr* (Voss and Smith 2005). We show here that *ngfr* and *met1* map to a genomic region that was structured by chromosomal rearrangements after the divergence of salamanders and anurans from a common ancestor. As a result, a unique set of *met1* region genes were brought together during evolution, and several of these encode proteins that function in related biological processes. Further, several genes in linkage disequilibrium with the *met1* region are differentially expressed in the brain during larval development, indicating that more than one gene from the *met1* region may explain phenotypic differences between these species. At a genomic level, more than 200 genes, including genes that code for proteins with mitochondrial functions, were differentially expressed between *met1* genotypes that significantly affect metamorphic timing. These changes were observed during a specific interval of time late in the larval period in interspecific hybrids, but at a much earlier time in the parental species. Our results show that *met1* regulates temporal changes in brain transcription during larval development and the timing of metamorphosis, but not the rate of larval growth preceding these events.

Materials and Methods

Salamander Care and Genotyping

Second-generation hybrids were generated by backcrossing an *A. t. tigrinum*–*A. mexicanum* F_1 hybrid male to an *A. mexicanum* female via in vitro fertilization (Voss 1995). Embryos were transferred to large containers of pond water and

aerated. Hatching was synchronized manually and from hatching onward, larvae were reared individually. From hatching until approximately 21 days posthatching (DPH), larvae were fed brine shrimp napuli (*Artemia*). After this, larvae were fed California blackworms (*Lumbriculus*). At 19 DPH, tail clippings were collected for genomic DNA extraction using phenol/chloroform. Genotyping was performed to determine whether individuals were carrying *A. mexicanum*, *A. t. tigrinum*, or a combination of species-specific alleles at loci from the *met1* genomic region. Genotypes for several loci (discussed later) were obtained using AcycloPrime-FP chemistry and a Wallac Victor3 plate reader as described in Smith et al. (2005). The polymerase chain reaction primers and extension probes that were used to type *met1* region loci are presented in supplementary table S1, Supplementary Material online.

At 28, 42, 56, 70, 84, 98, and 112 DPH, 18 unique individuals were measured for snout-vent length (SVL) prior to tissue harvesting (i.e., no individual was measured more than once). Whole brains and pituitaries were then removed and immediately flash frozen in liquid nitrogen (six of each *met1* genotype per time point). Excluding two recombinants (one at 70 DPH and one at 112 DPH), half of these individuals were homozygous for axolotl alleles across *ngfr*, *rasd1*, *map2k3*, *rai1*, and *shmt1* (i.e., had a $met1^{mex/mex}$ genotype), whereas the other half were heterozygous for these loci (i.e., had a $met1^{mex/Att}$ genotype). An additional 30 animals, including one recombinant ($ngfr^{mex/Att}$, $rasd1^{mex/mex}$, $map2k3^{mex/Att}$, $rai1^{mex/mex}$, and $shmt1^{mex/mex}$), were allowed to develop indefinitely, so that we could examine the relationship between *met1* genotype and metamorphic timing. All animal care and use procedures were in accordance with protocols approved by the University of Kentucky Institutional Animal Care and Use Committee.

Comparative and QTL Mapping of *met1*

Previously, we performed *A. mexicanum*/*A. t. tigrinum* × *A. mexicanum* backcrosses and developed markers from ESTs to make linkage maps (Voss 1995; Voss and Shaffer 1997, 2000; Voss and Smith 2005; Voss et al. 2011). In this study, we used the mapping panel and markers from Voss et al. (2011) to perform genome-wide QTL scans for metamorphic timing QTL. Genome-wide marker information is detailed in Voss et al. (2011). Marker orders were determined using MultiPoint 2.2 (MultiQTL Ltd., Hafia, Israel) and the Kosambi mapping function (Kosambi 1944). QTL were identified using R/qtl (Broman et al. 2003), the scanone function, the normal QTL model, and Haley–Knott regression (Haley and Knot 1992). Genome-wide thresholds for evaluating the significance of QTL were determined from 1,000 replicated data sets (Churchill and Doerge 1994). We also used the mapping panel from Voss and Smith (2005) to map additional loci and more finely map the position of *met1*. Primer sequences, diagnostic polymorphisms, and polymorphism detection assays for *met1* region loci are summarized in supplementary table S1, Supplementary Material online.

Statistical Analyses of Growth and Metamorphic Timing in Backcrossed Hybrids

We assessed whether backcrossed hybrids with nonrecombinant heterozygous and homozygous genotypes for *ngfr*, *rasd1*, *map2k3*, *rai1*, and *shmt1* differed in growth trajectory by fitting a general linear model of the following form: $SVL_{tij} = \beta_t + G_t + T_i + (GT)_{ti} + T^2{}_i + (GT^2)_{ti} + \varepsilon_{tij}$, where β_t is the intercept for $met1^{mex/mex}$ individuals, G_t is the difference between the intercept for $met1^{mex/mex}$ and $met1^{mex/Att}$ individuals, T_i is the linear regression coefficient for $met1^{mex/mex}$ individuals, $(GT)_{ti}$ is the difference between the linear regression coefficients for $met1^{mex/mex}$ and $met1^{mex/Att}$ individuals, $T^2{}_i$ is the quadratic regression coefficient for $met1^{mex/mex}$ individuals, $(GT^2)_{ti}$ is the difference between the quadratic regression coefficients for $met1^{mex/mex}$ and $met1^{mex/Att}$ individuals, and ε_{tij} is the error term for the *j*th individual of genotype *t* (a dummy variable) sampled at time *i*. This error term is assumed to be normally distributed with mean = 0 and variance = σ^2 and describes the deviation of each individual (irrespective of genotype) from its expected value based on the fitted model, which accounts for systemic differences between the genotypes when making predictions. A backward selection procedure was then applied in which parameters with *t*-statistic *P* values $\geq$ 0.05 and deletion test *P* values $\geq$ 0.05 were removed from the model (Crawley 2007). When conducting this procedure, the quadratic interaction term between genotype and time (i.e., $(GT^2)_{ti}$) was removed prior to the linear interaction term between genotype and time (i.e., $(GT)_{ti}$), which was removed prior to the main effect of genotype (i.e., G_t). We also assessed whether biphasic salamanders that were nonrecombinant for *ngfr*, *rasd1*, *map2k3*, *rai1*, and *shmt1* differed in time to completion of metamorphosis by conducting a one-tailed Mann–Whitney test. Salamanders that did not complete metamorphosis within 365 DPH were scored as paedomorphs.

RNA Extraction, Microarray Platform, and Quality Control

Total RNA was extracted individually from the brains of backcrossed hybrids sampled between 42 and 112 DPH. RNA extractions were conducted using TRIzol (Invitrogen) according to the manufacturer's protocol. Samples were further purified using RNeasy mini columns (Qiagen). Upon extraction, RNA samples were quantified via UV spectrophotometry and qualified via an Agilent Bioanalyzer. Four RNA samples per genotype (i.e., nonrecombinant homozygotes vs. heterozygotes) from each of six time points (42, 56, 72, 84, 98, and 112 DPH) were submitted to the University of Kentucky Microarray Core Facility (UKMCF). The UKMCF generated biotin-labeled cRNA targets for each of the 48 samples and

independently hybridized each sample to a custom *Ambystoma* Affymetrix GeneChip (Page et al. 2007). This microarray platform consists of 4,844 probe sets that were designed using a preferred maximum of 11 probe pairs (match/mismatch) and a possible minimum of 8 probe pairs. Of these 4,844 probe sets, 57 are Affymetrix controls, 4,596 were designed from *A. mexicanum* sequence, and 191 were designed from *A. t. tigrinum* sequence. We subjected all microarray data to low-level quality control (QC) as described previously (Page et al. 2010) and used the robust multiarray average (RMA) algorithm (Irizarry et al. 2003) to generate probe set-level expression summaries. We then examined the probe set-level data by computing correlation matrices for replicate GeneChips, conducting principal component analysis, and rendering pair-wise M versus A plots of replicate GeneChips. Upon conducting low-level and probe set-level QC, it was clear that one of the $met1^{mex/mex}$ 42 DPH GeneChips was aberrant. Thus, this GeneChip was removed prior to further processing and analysis. All QC analyses were performed using the R statistical computing environment (www.r-project.org, last accessed July 16, 2013) and the affy and affyPLM packages (Gautier et al. 2004; Bolstad et al. 2005). All sequence data, the raw microarray data (.CEL files), and the microarray annotations are available at Sal-Site (http://www.ambystoma.org/genome-resources, last accessed September 17, 2013).

Identification of Zero Mismatch Probe Sets and Expression Summarization

Despite the shallow phylogenetic distance between *A. mexicanum* and *A. t. tigrinum* (Shaffer and McKnight 1996; O'Neill et al. 2013), it is possible that targets from backcrossed hybrids will have variable hybridization efficiencies for probes on the *Ambystoma* GeneChip due to sequence divergence between the parent species (Bar-Or et al. 2007; Buckley 2007). To address this issue, we used probe sequences as queries in Blast searches of *A. mexicanum* and *A. t. tigrinum* EST contig databases. Blast alignments were then used to extrapolate the number of mismatches between each probe's sequence and *A. mexicanum* and *A. t. tigrinum* EST-based contigs, respectively (Page et al. 2010). In total, 1,604 probe sets (~33%) were designed from contigs with predicted orthologs in *A. mexicanum* and *A. t. tigrinum*, and for 1,320 (~82%) of these, we did not detect any mismatches between the evaluated probe sequences and the contig sequence from the heterologous species. However, for 31 of these probe sets (~2%), we were only able to assess a subset of the probes, and we therefore refer to these probe sets as equivocal zero mismatch probe sets (EZMMPSs) to distinguish them from the 1,289 zero mismatch probe sets (ZMMPSs) that were fully evaluated. Upon completing this exercise, we used the subset option of the RMA function in the affy package to calculate probe set-level expression summaries based on the 1,320 ZMMPSs and EZMMPSs and used this RMA matrix to identify differentially expressed genes (DEGs; discussed later).

Statistical Analysis of Microarray Data

To arrive at a list of DEGs, we implemented two statistical approaches. First, the limma package (Smyth 2004) was used to compare the alternate *met1* genotypes at 42, 56, 70, 84, 98, and 112 DPH. This involved fitting a linear model to each probe set that contained 12 coefficients, one for each time by genotype combination. We then reoriented this model in terms of contrasts between the two genotypes at each of the six time points. We corrected for multiple testing by applying a 0.05 false discovery rate (Benjamini and Hochberg 1995) to the *P* values associated with the moderated *F* statistics that resulted from our contrast matrix. In addition, for some downstream analyses, we required that DEGs identified using limma be differentially regulated by $\geq$1.5-fold as a function of *met1* genotype at one or more time points.

To identify genes with modest but temporally consistent expression differences between the *met1* genotypes, we also used the maSigPro package to conduct a stepwise quadratic regression analysis (Conesa et al. 2006). We corrected for multiple testing by applying a 0.05 false discovery rate (Benjamini and Hochberg 1995) at the overall model level. We then implemented a backward selection procedure (Conesa et al. 2006) that removed parameters from the full quadratic model with *P* values > 0.001, a stringent threshold that better enabled us to exclude genes with modestly different temporal trajectories between *met1* genotypes, but little to no difference in elevation (i.e., expression levels). We also required that models have $R^2 \geq 0.50$ and significant genotype, genotype by time, or genotype by time^2 terms. Finally, we graphically inspected the 96 genes that met the above criteria and manually selected genes that were robustly different between the alternate *met1* genotypes at several time points.

Enrichment Analyses

We used EASE analyses, as implemented by DAVID (Dennis et al. 2003), to identify biological process, cellular component, and molecular function gene ontology terms that were statistically enriched in lists of DEGs. This approach applies a conservative adjustment to the calculation of Fisher's exact probability from a hypergeometric distribution (Hosack et al. 2003). The ZMMPSs and EZMMPs with predicted orthologies to human proteins were used to generate expected values (i.e., as the background). The count threshold was set to two, and the EASE threshold (i.e., the critical value of the corrected Fisher's exact *P* value) was set to 0.05.

Examination of Hybrid DEG Expression in the Parent Species

In a previous study, we used the same microarray platform used here to investigate neurodevelopmental gene expression in *A. mexicanum* and *A. t. tigrinum* at 42, 56, 70, and 84 DPH (Page et al. 2010). We used the raw data from this prior experiment (i.e., the .CEL files) to generate a zero mismatch RMA matrix for the parent species that is analogous to the zero mismatch RMA matrix for backcrossed hybrids described earlier. We then obtained $\log_2$(RMA) values from this matrix for probe sets that were identified as differentially expressed between $met1^{mex/mex}$ and $met1^{mex/Att}$ hybrids in this study using limma. For each of these probe sets, we used Welch's *t* statistic to test for differential expression between *A. mexicanum* and *A. t. tigrinum* at each time point that we sampled parental gene expression (Page et al. 2010). In addition, we used Kruskal's nonmetric multidimensional scaling (NMDS) to examine relationships among hybrid, *A. mexicanum*, and *A. t. tigrinum* expression for DEGs that differed between the hybrid *met1* genotypes by $\geq$1.5-fold at one or more time points (Venables and Ripley 2010). NMDS is an ordination technique for dimension reduction that can be used on any measure of dissimilarity (i.e., distance). It uses an iterative regression-based approach to find a numerical solution for representing the distance relations among observations from a high dimensional data set in *k* dimensions, where *k* is a small number relative to the dimensionality of the original data set. NMDS is nonmetric in the sense that it only attempts to maintain the rank order of distances in the spatial representation. The stress is a common statistic for assessing the fit of an NMDS solution (Venables and Ripley 2010) that can be interpreted as a measure of the distortion in the distance relationships that results from dimension reduction. When conducting NMDS, we used $1 - r$ as a measure of dissimilarity where *r* is Pearson's correlation coefficient. This measure of dissimilarity ensures that all distances fall between zero and two and that the correlation across genes between samples determines the magnitude of dissimilarity, with positively correlated samples treated as similar and negatively correlated samples treated as dissimilar. We allowed a maximum of 150 iterations and conducted NMDS for $k = 1$–10 dimensions to examine how the stress changed as a function of the number of dimensions used for ordination.

Results

Effect of *met1* Genotype on Larval Growth and Metamorphic Timing in Backcrossed Hybrids

Of the 30 individuals allowed to develop indefinitely, only two $met1^{mex/mex}$ individuals failed to metamorphose within 365 days and were thus scored as paedomorphs. The single recombinant for the *met1* region ($ngfr^{mex/Att}$, $rasd1^{mex/mex}$, $map2k3^{mex/Att}$, $rai1^{mex/mex}$, and $shmt1^{mex/mex}$) completed metamorphosis at a relatively early time (164 DPH), consistent with *met1* associating more closely with *map2k3* and *ngfr* than the other loci (discussed later). Twenty-seven individuals that were nonrecombinant for the *met1* region metamorphosed. Among these, a highly statistically significant difference in metamorphic timing was observed between $met1^{mex/mex}$ and $met1^{mex/Att}$ individuals (fig. 1*A*). Despite this pronounced difference in metamorphic timing, there was no difference between the *met1* genotypes in larval growth trajectory throughout the time period that tissues were collected (table 1 and fig. 1*B*). These results show that *met1* affects the timing of metamorphosis and the probability of expressing paedomorphosis without affecting early larval growth rate.

Comparative and QTL Mapping of *met1*

Previous studies identified *ngfr* as the closest protein-coding marker to *met1* in the *Ambystoma* genetic linkage map (Smith et al. 2005; Voss and Smith 2005). To obtain linked markers for *ngfr*, we scanned genomic regions flanking *ngfr* in the *Homo sapiens* and *Gallus gallus* genomes and then selected loci that were good candidates for *met1*. This strategy was not very successful because the *ngfr* chromosome in *H. sapiens* (*Hsa17*) has undergone considerable rearrangement during evolution and the *ngfr* chromosome in *G. gallus* (*Gga28*) contains a *ngfr*-like gene sequence that does not show high sequence identity to the *Ambystoma* ortholog. We eventually mapped *map2k3* to within 5 cM of *ngfr*, an unexpected result because *map2k3* is approximately 2.6×10^7 bases from *ngfr* in the human genome and these loci occur on different chromosomes in the chicken genome (fig. 2*A*). Linkage of *map2k3-ngfr* implicated a new set of candidate genes for *met1* and, in particular, genes from the Smith–Magenis syndrome (SMS) genomic region (*Hsa*17p11.2). Four additional loci (*rasd1*, *rai1*, *shmt1*, and *drg2*) were subsequently mapped to establish linkage of SMS loci to *map2k3*. Several genes were then mapped within 5 cM on the opposite flank of *ngfr*, including *setd2*, *c11orf51*, *ccm2*, *kif9*, and *aurkb*. All of these genes except *aurkb* are syntenic within the same genomic scaffold in *Xenopus tropicalis*, and *setd2* and *ccm2* are linked on chromosome 2 in *G. gallus*. However, the *ngfr-setd2-c11orf51-ccm2-kif9* conserved synteny group does not locate to the SMS conserved synteny group in the *X. tropicalis* genome, nor are these genes found together in fish or amniote genomes. These results show that *ngfr* and *map2k3* flank the position of an ancestral chromosomal breakpoint that is not observed in representative anuran (*Xenopus*) and reptile (*Gallus*) genomes and therefore may be unique to *Ambystoma* and possibly other salamanders (fig. 2*A*).

The most likely position of *met1* was determined by QTL analysis using two different mapping panels: LAB ($N = 90$) and WILD2 ($N = 496$). In LAB, the segregation of discrete metamorphic and paedomorphic phenotypes was observed to be largely consistent with a single gene model of inheritance

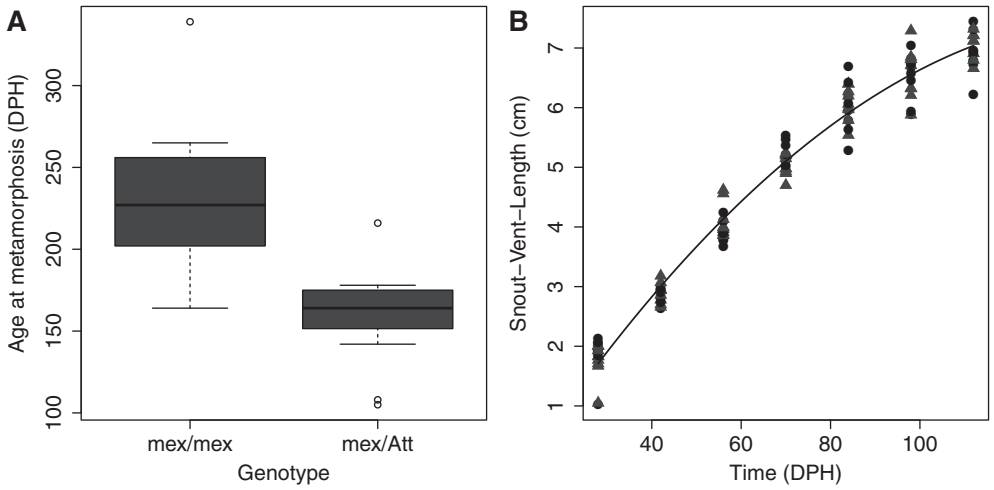

Fig. 1.—(*A*) Box plots comparing the ages at which spontaneous metamorphosis was completed by biphasic $met1^{mex/mex}$ ($n = 8$) and $met1^{mex/Att}$ ($n = 19$) hybrids. The difference in metamorphic timing between the alternate *met1* genotypes is highly statistically significant (one-sided Mann–Whitney test, $W = 142.5$, $P = 0.0002$). (*B*) Scatter plot comparing the growth trajectories of $met1^{mex/mex}$ hybrids (black circles) and $met1^{mex/Att}$ hybrids (gray triangles). The six parameter dummy variable regression model described in Materials and Methods and table 1 was fit to the data. Stepwise deletion tests revealed that retaining a separate quadratic regression coefficient ($F_{1,118} = 0.051$, $P = 0.822$), a separate linear regression coefficient ($F_{1,119} = 0.858$, $P = 0.356$), and a separate intercept ($F_{1,120} = 0.083$, $P = 0.774$) for $met1^{mex/Att}$ hybrids was not necessary. Thus, the curve shown corresponds to the selected model ($F_{2,121} = 2{,}181$, $P \ll 0.0001$) and implies that there is no difference between the growth trajectories of the alternate *met1* genotypes.

Table 1

Parameter Estimates, *t* Statistics, *t* Statistic *P* Values, and Adjusted R^2 Values for the Models Fit During the Selection Procedure Used to Compare the Growth Trajectories of $met1^{mex/mex}$ and $met1^{mex/Att}$ Hybrids

Estimate	Full Model	Step 1	Step 2	Step 3
$B_t \pm$ SE	$-1.34 \pm 2.57 \times 10^{-1}$	$-1.30 \pm 1.96 \times 10^{-1}$	$-1.36 \pm 1.83 \times 10^{-1}$	$-1.36 \pm 1.81 \times 10^{-1}$
B_t *t* value	−5.19	−6.63	−7.46	−7.52
$P(B_t) = 0$	8.73×10^{-7}	1.03×10^{-9}	1.48×10^{-11}	1.05×10^{-11}
$G_t \pm$ SE	$-3.56 \times 10^{-2} \pm 3.64 \times 10^{-1}$	$-1.11 \times 10^{-1} \pm 1.47 \times 10^{-1}$	$1.57 \times 10^{-2} \pm 5.47 \times 10^{-2}$	Removed
G_t *t* value	−0.10	−0.75	0.29	Removed
$P(G_t) = 0$	0.92	0.45	0.77	Removed
$T_i \pm$ SE	$1.21 \times 10^{-1} \pm 8.15 \times 10^{-3}$	$1.20 \times 10^{-1} \pm 5.84$ x10^{-3}	$1.21 \times 10^{-1} \pm 5.74 \times 10^{-3}$	$1.21 \times 10^{-1} \pm 5.72 \times 10^{-3}$
T_i *t* value	14.88	20.55	21.09	21.18
$P(T_i) = 0$	$<2.00 \times 10^{-16}$	$<2.00 \times 10^{-16}$	$<2.00 \times 10^{-16}$	$<2.00 \times 10^{-16}$
$T^2_i \pm$ SE	$-4.20 \times 10^{-4} \pm 5.74 \times 10^{-5}$	$-4.11 \times 10^{-4} \pm 4.06 \times 10^{-5}$	$-4.12 \times 10^{-4} \pm 4.05 \times 10^{-5}$	$-4.12 \times 10^{-4} \pm 4.04 \times 10^{-5}$
T^2_i *t* value	−7.32	−10.13	−10.16	−10.21
$P(T^2_i) = 0$	3.28×10^{-11}	$<2.00 \times 10^{-16}$	$<2.00 \times 10^{-16}$	$<2.00 \times 10^{-16}$
$(GT)_{ti} \pm$ SE	$-7.44 \times 10^{-4} \pm 1.15 \times 10^{-2}$	$1.81 \times 10^{-3} \pm 1.96 \times 10^{-3}$	Removed	Removed
$(GT)_{ti}$ *t* value	−0.07	0.93	Removed	Removed
$P[(GT)_{ti}] = 0$	0.95	0.36	Removed	Removed
$(GT^2)_{ti} \pm$ SE	$1.83 \times 10^{-5} \pm 8.14 \times 10^{-5}$	Removed	Removed	Removed
$(GT^2)_{ti}$ *t* value	0.23	Removed	Removed	Removed
$P[(GT^2)_{ti}] = 0$	0.82	Removed	Removed	Removed
Adjusted R^2	0.9721	0.9723	0.9724	0.9726

Note.—To further emphasize the rationale used during the model selection process, additional decimal places are shown for adjusted R^2 relative to the other reported values.

(Voss 1995). Accordingly, binary QTL mapping was used to map *met1* in LAB. A genome-wide scan for QTL using approximately 900 markers identified only one locus on linkage group 2 (LG2) with LOD scores exceeding an empirically determined significance threshold (LOD > 3.35, $P = 0.05$; fig. 2*B*). The maximum LOD score obtained by interval mapping placed *met1* between conserved syntenies defined by *ngfr-setd2-kif9* and *map2k3-rasd1-rai1-shmt1* (fig. 2*C*).

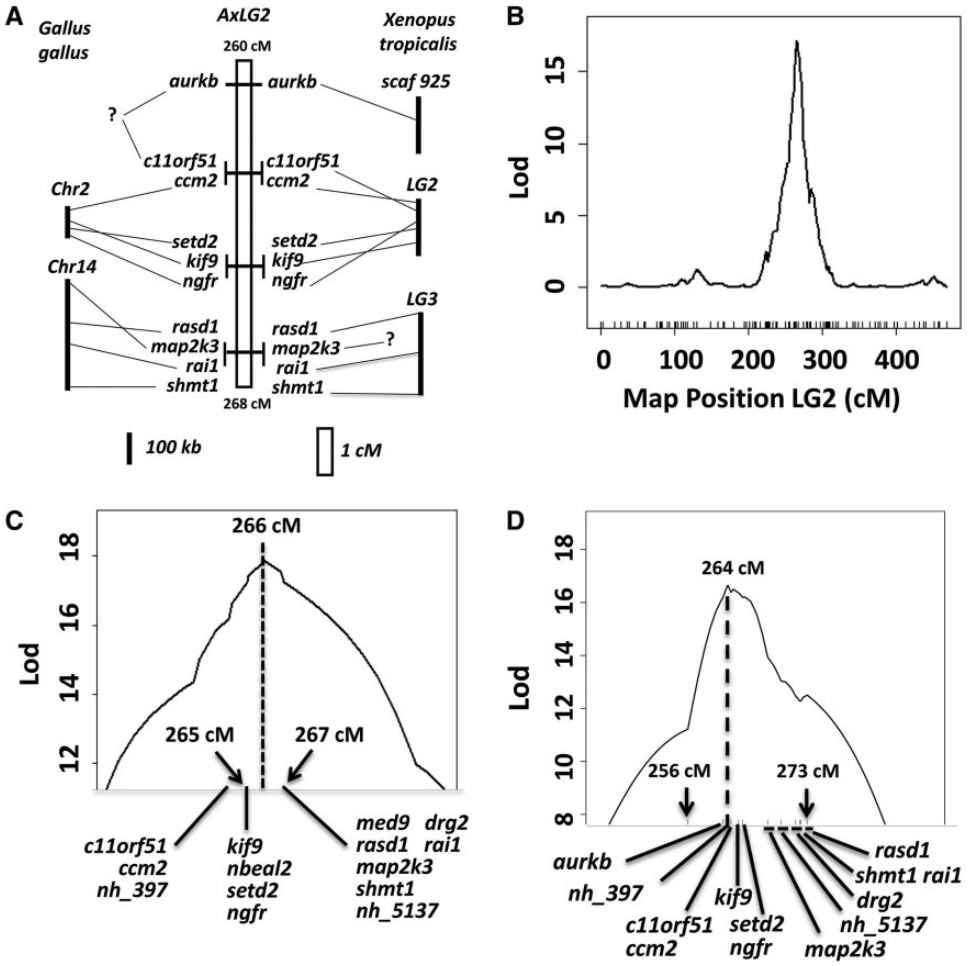

Fig. 2.—(*A*) Comparative map showing marker positions on *Ambystoma* linkage group 2 (*AxLG2*; center) and the positions of their orthologs in *Gallus gallus* (left) and *Xenopus tropicalis* (right). (*B*) Results of a genome-wide scan for life history pathway QTL (metamorphosis vs. paedomorphosis) using the LAB mapping panel. A single significant LOD peak corresponding to *met1* was identified on *Ambystoma* LG2. (*C*) Local map of the *met1* genomic region on LG2 based on the LAB mapping panel. (*D*) Result of a genome-wide scan for metamorphic timing QTL based on the WILD2 mapping panel. A single significant LOD peak corresponding to *met1* was identified on LG2.

However, this position is based on a single recombinant genotype, and the LOD is equivalent when estimated at the position of any of these flanking markers. To more accurately map *met1*, we turned to the larger WILD2 panel. In WILD2, we previously reported that ~90% of individuals showed continuous variation in metamorphic timing, and this variation was largely explained by *met1* (Voss and Smith 2005). Thus, we typed genes from the *met1* genomic region and performed QTL analysis of metamorphic timing to identify the most likely position for *met1* in WILD2. Gene orders were resolved to a finer degree using the WILD2 mapping panel (fig. 2*D*). The maximum LOD peak coincided with the position of an EST contig (*nh_397*) that is presumptively unique to *A. tigrinum* spp. because it does not show sequence identity to any NCBI nucleotide or protein-coding sequence. However, the LOD was approximately equivalent for a 3-cM interval defined by flanking genes *aurkb* and *setd2/ngfr*. The LOD score dropped approximately 2 LOD between *ngfr* and *map2k3* and declined further for other SMS loci, although a minor peak was observed at the position of *rasd1*. Under the assumption that *met1* corresponds to a single gene, the most likely position for this gene is between *aurkb* and *map2k3*.

Effect of *met1* Genotype on Gene Expression in Backcrossed Hybrids

We identified 187 ZMMPSs and 6 EZMMPSs that measured differential transcript abundance between the alternate *met1* genotypes at one or more time points using limma (supplementary table S2, Supplementary Material online). Thus, there is no statistical evidence that this list of DEGs is enriched with EZMMPSs (odds ratio = 1.41, lower 95% confidence limit = 0.47, upper 95% confidence limit = 3.59, *P*[odds ratio = 1] = 0.44). A few of these genes were identified as

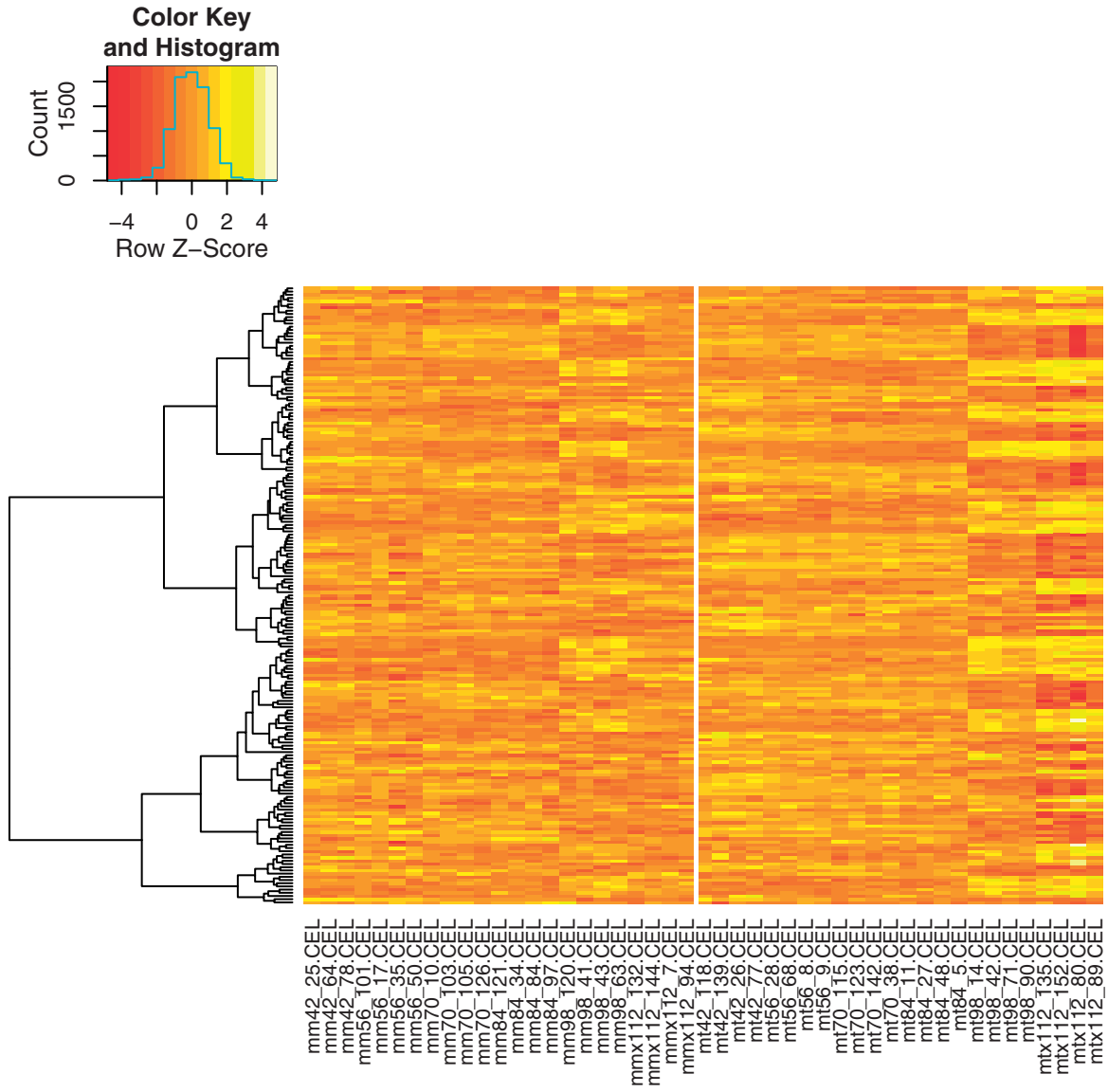

Fig. 3.—Heat map showing the row scaled data from the 193 genes identified using limma. The columns correspond to individual GeneChips with the prefixes mm and mt corresponding to *met1*$^{mex/mex}$ and *met1*$^{mex/Att}$ hybrids, respectively. The time points in DPH are denoted by the numbers immediately following the lettered prefixes. *Met1*$^{mex/mex}$ and *met1*$^{mex/Att}$ GeneChips are separated by a vertical white line. The dendrogram to the left was obtained via hierarchical clustering of a Euclidean distance matrix.

differentially expressed at the first five time points (42, 56, 70, 84, and 98 DPH), but most were differentially expressed at the last time point (112 DPH). A substantial proportion of these DEGs exhibited temporal changes in both genotypes between 84 and 98 DPH (fig. 3). However, between 98 and 112 DPH, most of these genes returned to expression levels similar to those observed between 42 and 84 DPH in *met1*$^{mex/mex}$ individuals (fig. 3). Conversely, the expression changes initiated between 84 and 98 DPH continued or intensified in *met1*$^{mex/Att}$ individuals (fig. 3). The dummy variable quadratic regression approach identified 93 ZMMPSs and 3 EZMMPSs that measured different temporal patterns of expression between the alternate *met1* genotypes (supplementary table S3, Supplementary Material online). Hence, there is also no statistical support for the idea that the DEGs identified via maSigPro are statistically enriched with EZMMPSs (odds ratio = 1.38, lower 95% confidence limit = 0.26, upper 95% confidence limit = 4.59, P[odds ratio = 1] = 0.49). Visual inspection of these 96 profiles identified 10 genes with robust expression differences between the alternate *met1* genotypes (table 2; supplementary fig. S1, Supplementary Material online). Two of the genes from this list map to LG2 (table 2), and 6 of the 13

Table 2
The 10 Genes Identified via Dummy Variable Regression and Graphical Inspection with Temporally Consistent Differences in mRNA Abundance between Backcrossed Hybrids with Alternate *met1* Genotypes

Gene	Probe Set ID	Sal-Site Version 3 ID
*Atp6v0c**	SRV_01135_a_at	Contig18638
Dhcr7	SRV_00879_s_at	Contig40972
Eif4a1	SRV_00923_a_at	Mex_NM_001416_Contig_9
Gdi2	SRV_00964_a_at	Mex_NM_001494_Contig_1
H2afy2	SRV_13464_a_at	Tig_NM_018649_Contig_1
Hdac2	SRV_02393_a_at	Contig40786
Hsp90b1	SRV_01812_a_at	Mex_NM_003299_Contig_6
NHO	SRV_09160_a_at	Contig77873
*Rac1**	SRV_03102_a_at	Contig20873
Tomm70a	SRV_03611_a_at	Contig02244

NOTE.—Sal-Site identifiers correspond to assembly version 3. Profiles of these genes are shown in supplementary figure S1, Supplementary Material online. NHO, no established human ortholog. Asterisk indicates genes that map to *Ambystoma* LG2.

DEGs identified from both statistical approaches that map to LG2, located within 35 cM of *met1*. These patterns indicate that *met1* genotype is associated with *cis* and *trans* transcriptional changes that commence late in the larval period, before morphological metamorphosis.

Met1 Is Associated with the Expression of Genes with Mitochondrial and Neurodevelopmental Functions

Amphibian metamorphosis depends on transcriptional activation of numerous biological processes that transform larval phenotypes into adult phenotypes (Shi 2000). Because our analyses suggested that the vast majority of *met1*'s transcriptional effects are exerted late in the larval period, we used genes that were differentially expressed between $met1^{mex/mex}$ and $met1^{mex/Att}$ hybrids at 112 DPH to identify biological processes associated with *met1*. As can be seen in table 3, DEGs upregulated in $met1^{mex/Att}$ hybrids at 112 DPH were highly enriched for genes that function in the mitochondria, with particular enrichment for genes associated with electron transport (supplementary table S4, Supplementary Material online). The 24 DEGs that mapped to the mitochondrion ontology term are associated with a variety of functions including protein synthesis (*mrpl13*, *mrpl30*, and *mrps7*), steroid metabolism (*hint2*), and apoptosis (*cycs*). In addition, six genes (*ndufa4*, *ndufa7*, *ndufab1*, *ndufc1*, *ucrc*, and *uqcrh*) associated with mitochondrial ATP synthesis coupled to electron transport were also upregulated in $met1^{mex/Att}$ hybrids at 112 DPH, indicating a change in mitochondrial energetics in individuals that metamorphosed (on average) at significantly earlier times. The DEGs that were upregulated in $met1^{mex/mex}$ individuals (i.e., the genes downregulated in $met1^{mex/Att}$ individuals) at 112 DPH were enriched with genes that mapped to a number of biological processes associated with the endomembrane system, translation, and neurodevelopment (table 3; supplementary table S5, Supplementary Material online). Of particular interest are several genes (*actb*, *mtpn*, *rhoa*, *rac1*, *rtn4*, and *ubc*) associated with neurogenesis in mammals that were upregulated in $met1^{mex/mex}$ hybrids relative to $met1^{mex/Att}$ hybrids. Collectively, these results suggest divergent patterns of brain development and function between $met1^{mex/mex}$ and $met1^{mex/Att}$ hybrids. In particular, $met1^{mex/Att}$ hybrids increase transcription of genes associated with mitochondrial bioenergetics at a time that precedes metamorphosis.

Expression of Hybrid DEGs in the Parent Species

In a previous study, we characterized growth rates and neurodevelopmental gene expression in *A. mexicanum* and *A. t. tigrinum* larvae from 42 to 84 DPH (Page et al. 2010). In that study, *A. t. tigrinum* larvae grew at a faster rate, and all *A. t. tigrinum* showed definitive signs of morphological metamorphosis by 84 DPH. Metamorphosis-associated genes were identified from *A. t. tigrinum* that changed in abundance as larval development proceeded, and these changes were particularly pronounced at the later time points. In addition, 419 probe sets with zero nucleotide mismatches between *A. mexicanum* and *A. t. tigrinum* measured consistently different magnitudes of expression between species, with expression generally higher in *A. t. tigrinum*. Reexamination of how the 193 DEGs identified from hybrids in this study using limma were expressed in the parent species revealed a robust pattern of gene expression divergence (fig. 4). The distribution of *P* values for the 772 *t* statistics we computed from the parental data differs greatly from the uniform distribution that would be expected if there were no expression differences between the species (fig. 5). This general pattern also holds for each time point when the *P* values are not pooled (not shown). Approximately 65% of these genes were differentially expressed ($\alpha = 0.05$) between *A. mexicanum* and *A. t. tigrinum* at one or both of the two earliest time points (42 or 56 DPH). Moreover, approximately 78% of these genes were differentially expressed between the parent species ($\alpha = 0.05$) at one or more of the four time points that we sampled parental gene expression. These results show that many of the genes that are differentially expressed as a function of *met1* genotype at 112 DPH in backcrossed hybrids are also differentially expressed between *A. mexicanum* and *A. t. tigrinum*, and that many of these differences are detectable in the parent species early during the larval period.

To visualize the degree of similarity in expression between hybrid *met1* genotypes and the parent species, we conducted NMDS on the 24 DEGs that were differentially expressed between $met1^{mex/mex}$ and $met1^{mex/Att}$ hybrids by $\geq$1.5-fold at one or more time points. The algorithm converged within 150 iterations for solutions in $k = 2$–10 dimensions. As can be seen in figure 6*A*, the stress did not level off until *k* was beyond a number of dimensions that could be easily

Table 3

Gene Ontology Terms that Were Significantly Enriched in Genes that Were Differentially Up and Downregulated in *met1*$^{mex/Att}$ Hybrids Relative to *met1*$^{mex/mex}$ Hybrids

GO ID	GO Term	*N*	*P*	Total	Enrichment
GO terms enriched in the DEGs upregulated in *met1*$^{mex/Att}$ hybrids at 112 DPH					
0005743	Mitochondrial inner membrane	17	2.32×10^{-6}	58	3.70
0022900	Electron transport chain	9	2.39×10^{-5}	18	6.24
0005739	Mitochondrion	24	2.17×10^{-4}	143	2.12
0006119	Oxidative phosphorylation	9	2.72×10^{-4}	24	4.68
0015078	Hydrogen ion transmembrane transporter activity	8	4.92×10^{-4}	21	5.01
0003735	Structural constituent of ribosome	13	9.44×10^{-4}	60	2.85
0042775	Mitochondrial ATP synthesis coupled electron transport	6	3.06×10^{-3}	14	5.35
0016491	Oxidoreductase activity	13	0.01	79	2.16
0015980	Energy derivation by oxidation of organic compounds	7	0.02	29	3.01
0006414	Translational elongation	10	0.03	57	2.19
0051234	Establishment of localization	25	0.03	213	1.46
0006120	Mitochondrial electron transport, NADH to ubiquinone	4	0.04	10	4.99
GO terms enriched in the DEGs downregulated in *met1*$^{mex/Att}$ hybrids at 112 DPH					
0012505	Endomembrane system	14	2.13×10^{-4}	69	3.10
0008135	Translation factor activity, nucleic acid binding	6	0.01	22	4.11
0003924	GTPase activity	7	0.01	31	3.41
0022008	Neurogenesis	6	0.02	25	3.59
0006417	Regulation of translation	5	0.03	19	3.94

NOTE.—In total, 70 gene ontology terms were enriched in the list of DEGs that were upregulated in *met1*$^{mex/Att}$ hybrids and 32 gene ontology terms were enriched in the list of DEGs that were downregulated in *met1*$^{mex/Att}$ hybrids. The data in the table correspond to a subset of these results, which are shown in their entirety in supplementary tables S4 and S5, Supplementary Material online. *P* = modified Fisher's exact *P* value. *N* = the number of DEGs that annotate to a given ontology term. Total = the number of genes on the array that annotate to a given ontology term. Enrichment = the increase in DEGs annotating to a given ontology term relative to the number of genes expected given a random draw from the array of equal size.

visualized. Nevertheless, there are several features of the NMDS solutions where $k = 2$ (fig. 6*B*) and $k = 3$ (fig. 6*C*) that suggest there is: 1) hybrid intermediacy in gene expression, 2) a change in both hybrid *met1* genotypes at 98 DPH that causes their expression profiles to more closely resemble *A. t. tigrinum* expression along at least one dimension, and 3) a reversal of the temporal trajectory initiated between 84 and 98 DPH in *met1*$^{mex/mex}$ hybrids that is not observed in *met1*$^{mex/Att}$ hybrids (fig. 3). When $k = 3$, these patterns are readily apparent in the values obtained for the horizontal axis depicted in figure 6*C*. The distributions of the coordinates for this dimension are shown for several developmentally relevant groups in figure 6*D*. Collectively, our reexamination of hybrid DEGs in the parental species suggests that many differences between *A. mexicanum* and *A. t. tigrinum* in neurodevelopmental gene expression trace to genetic factors from the *met1* genomic region.

Discussion

Evolutionary History of the *met1* Genomic Region

An important objective in evolutionary genetics is to identify genes for adaptive traits (Feder and Mitchell-Olds 2003). This objective has been pursued most often by testing a priori selected candidate genes (Voss et al. 2000, 2003), with fewer studies using unbiased approaches to identify candidate genes for QTL. A logical first step in searching for candidate genes is to cross-reference a QTL genomic region to a reference genome or genetic map. In our case, some of the *met1*-associated genes that we initially mapped were not found to be syntenic in any vertebrate genome. Through trial and error mapping of candidate loci and application of a functional genomics approach, we efficiently identified genes linked to *met1*. In the process, we obtained a sufficient number of loci to reconstruct the dynamic and lineage-specific history of chromosomal rearrangements that structured LG2 and the *met1* genomic region. LG2 primarily contains three ancestral blocks of loci that correspond to ancestral vertebrate chromosomes (Voss et al. 2011). In the chicken genome, these blocks correspond to *Gga12*, *Gga14*, and a portion of chicken chromosome 2 (*Gga2*). Genes from these three blocks are not syntenic in *Xenopus* and thus were fused after the divergence of anurans and salamanders from a common ancestor. During salamander phylogenesis, intrachromosomal rearrangements occurred between segments corresponding to *Gga2* and *Gga14*, interleaving conserved syntenic groups of loci and creating unique gene orders. This is uncharacteristic of the *Ambystoma* genome, which has undergone a lower overall chromosomal rearrangement

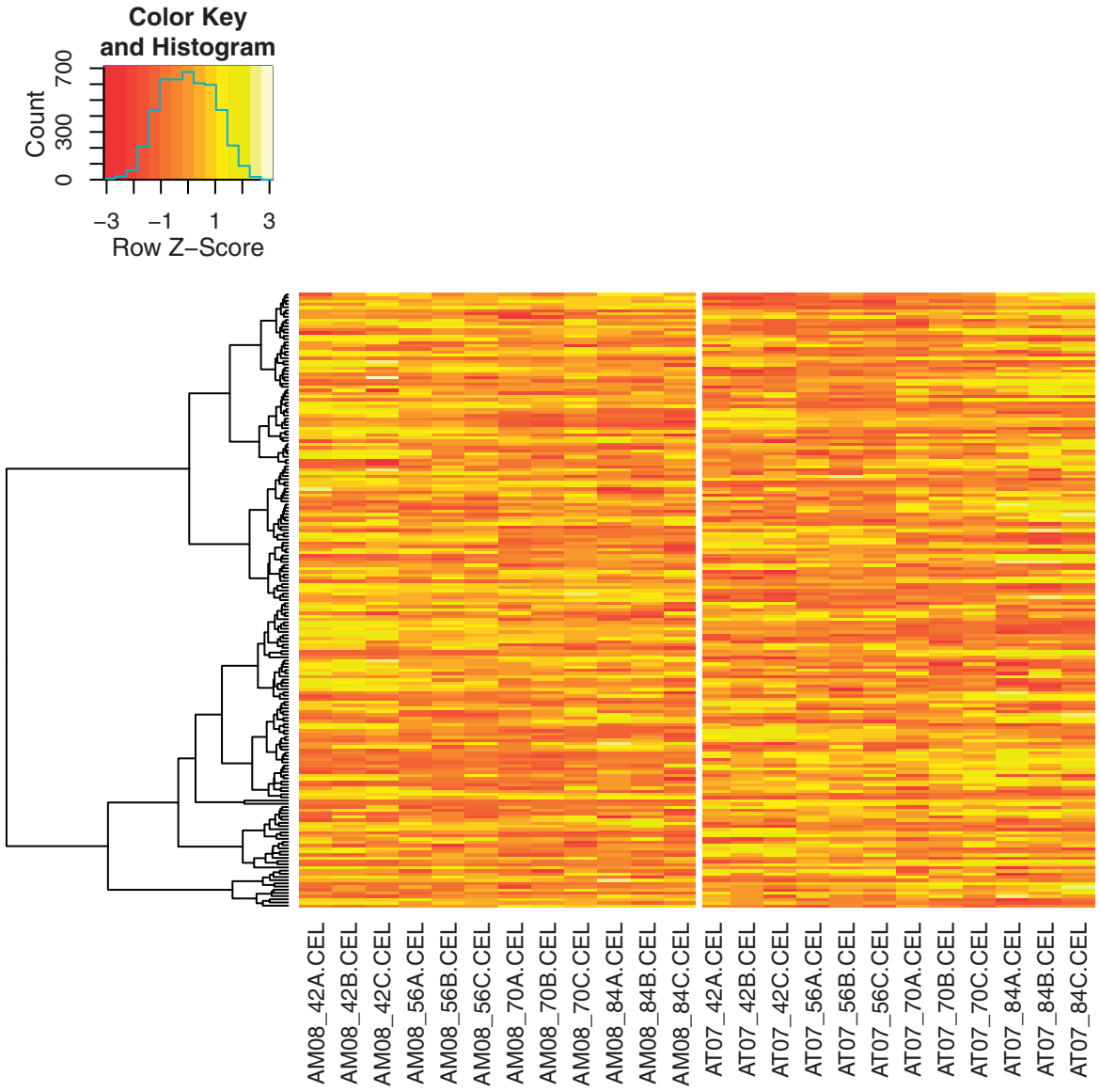

Fig. 4.—Heat map showing row scaled data from the parent species for the 193 genes identified from backcrossed hybrids using limma. The columns correspond to individual GeneChips with the prefixes AM and AT corresponding to *A. mexicanum* and *A. t. tigrinum* samples, respectively. The time points in DPH are denoted by the numbers immediately following the underscore. GeneChips from different species are separated by a vertical white line. The dendrogram to the left was obtained via hierarchical clustering of a Euclidean distance matrix.

rate than other vertebrates and especially mammals (Smith and Voss 2006). In fact, the chromosome associated with LG2 contains more lineage-specific, intrachromosomal rearrangements than are predicted from any other *Ambystoma* linkage group (Voss et al. 2011). Additional comparative mapping studies are needed to determine whether this chromosomal evolutionary history is unique to *A. tigrinum* spp. or shared among all extant salamanders. Of particular relevance to this study is the fact that these chromosomal rearrangements brought several genes with associated functions into linkage during evolution.

Gene Expression and the *met1* Genomic Region

Our functional genomics approach accomplished two important objectives. First, by comparing the abundances of RNAs between individuals that inherited different *met1* genotypes, we efficiently identified expression differences for loci linked to *met1*. Second, by comparing transcription within developing larval brains, we identified expression differences that are functionally associated with species-specific differences, including life history variation. Although it remains possible that *met1* corresponds to a single gene, the observation that several genes in linkage disequilibrium with *met1* were

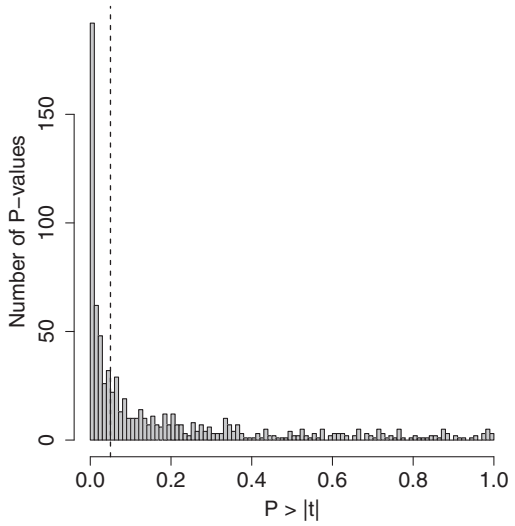

Fig. 5.—Histogram showing the distribution of the 772 *t* statistic *P* values that were calculated from previously generated data on *A. mexicanum* and *A. t. tigrinum*. The dashed vertical line denotes $P > |t| = 0.05$.

differentially expressed raises the possibility that more than one gene underlies the effect of *met1* on metamorphic timing and gene expression. Moreover, when considering genes mapped in this study, and other genes that are predicted by synteny to map to the reconstructed *met1* region, we find that several sets of functionally associated genes were brought into linkage during evolution. These include genes associated with brain development (*ngfr*, *ccm2*, *setd2*, *cspg5*, and *rasd1*), transcriptional regulation (*setd2*, *smarcc1*, *spop*, and *med9*), lipid biosynthesis (*srebf1*, *scap*, and *pemt*), and mitochondrial function (*tmem11*, *atpaf2*, and *nt5m*). Notably, *srebf1* and *scap* encode proteins that physically interact to regulate transcription of genes associated with cellular lipid homeostasis (Brown and Goldstein 1999). Linkage of functionally associated genes suggests that *met1* presents characteristics of a supergene. A supergene is a group of linked loci that cosegregate alleles for specifying suites of coadapted traits (Joron et al. 2006). In the case of *met1*, genes that were brought into linkage may specify multiple brain phenotypic differences between metamorphic *A. t. tigrinum* and paedomorphic *A. mexicanum*. It will be interesting to test the idea that *met1* is a supergene in natural populations where tiger salamanders express metamorphosis or paedomorphosis as a polymorphism to exploit ephemeral and permanent ponds, respectively.

Although it is unknown which mechanism functions in *A. mexicanum* to yield a paedomorphic developmental outcome, a recent study showed that *met1* is a TH-responsive QTL (Voss et al. 2012). We extend this finding to hypothesize that *met1* affects the brain's response to TH during development, and as a result, this causes variation in transcription and timing of metamorphosis. We observed a large number of genes that were expressed differently between the hybrid *met1* genotypes by 112 DPH, and many of these DEGs were also differentially expressed between *A. mexicanum* and *A. t. tigrinum* as early as 42 DPH and extending to 84 DPH. It is well established that TH activates new patterns of gene expression during anuran metamorphosis and vertebrate brain development (Shi 2000), including changes in cellular metabolism not unlike the highly enriched mitochondrial biological processes that we observed in our study. In particular, genes that function in electron transport and ATP synthesis were enriched in our study, suggesting a critical role for oxidative phosphorylation in meeting the energetic demands associated with neuronal differentiation and developmental processes that occur during metamorphosis. Overall, our results show that high and low brain bioenergetics profiles are established very early in the larval period between *A. t. tigrinum* and *A. mexicanum*, but later in the case of hybrids. This may explain why these species show different larval growth rates and life history outcomes.

Growth, Differentiation, and Metamorphic Timing

The timing of metamorphosis is an ecologically and evolutionarily important trait because it is influenced by temporal aspects of environmental factors that determine whether and when the adult habitat will become more suitable for growth and reproduction than the larval habitat. Consequently, the earliest and most influential ecological model of amphibian metamorphosis proposed that an organism's growth history is a critical determinant of metamorphic timing (Wilbur and Collins 1973). According to this model, there is a range of body sizes in which metamorphosis occurs, and within this range, metamorphosis will not proceed until the growth rate drops below a threshold value. Although there is strong empirical support for the idea that a threshold model is the appropriate framework for conceptualizing metamorphic timing (Morey and Reznick 2000), there is debate over whether growth rate or differentiation rate, two traits that are often highly correlated, is the crucial determinant (Smith-Gill and Berven 1979). At 112 DPH, we observed large-scale differences in transcription between *met1* genotypes that were not preceded by differences in growth rate. Moreover, many of these differences in gene expression appear to be associated with metamorphic differentiation events that are eminent in $met1^{mex/Att}$ hybrids, but not $met1^{mex/mex}$ hybrids. Although the relevance of our findings remains to be established for natural populations, our results show that differences in metamorphic timing are not necessarily coupled to differences in larval growth history.

Conclusion

We showed in this study that *met1* locates to a region of the *Ambystoma* linkage map that has been structured by

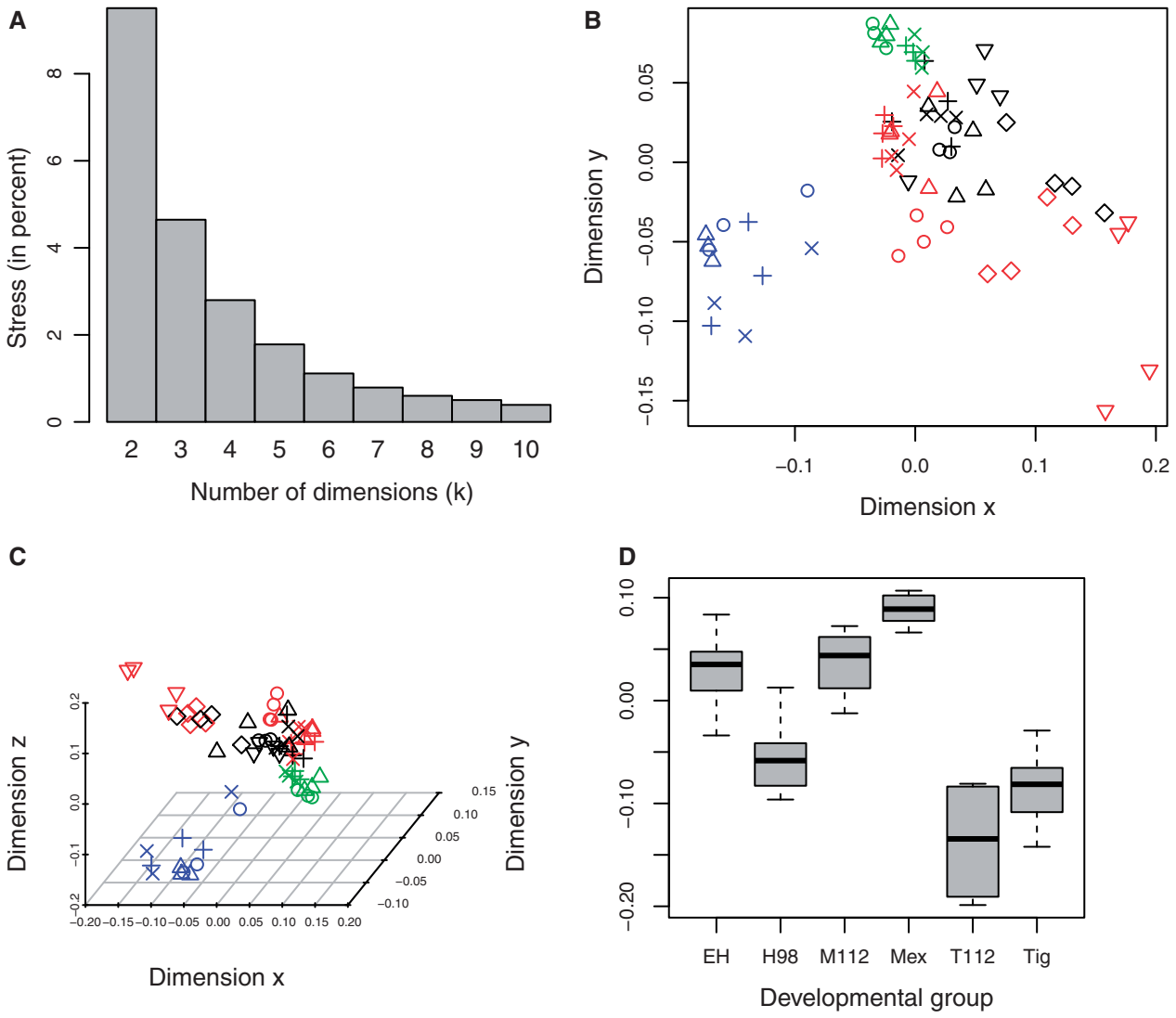

Fig. 6.—Results of the NMDS analysis: (*A*) scree plot showing the stress (in percent) for NMDS solutions based on different numbers of dimensions, (*B*) scatter plot of the coordinates obtained when $k = 2$, (*C*) scatter plot of the coordinates obtained when $k = 3$, and (*D*) box plots of various developmental groups' coordinates for the horizontal dimension shown in (*C*). In (*B*) and (*C*), green indicates *A. mexicanum*; blue, *A. t. tigrinum*; black, *met1*$^{mex/mex}$ hybrids; red, *met1*$^{mex/Att}$ hybrids. Circles = 42 DPH; triangles = 56 DPH; + = 70 DPH; × = 84 DPH; diamonds = 98 DPH; and inverted triangles = 112 DPH. In (*D*), EH = 42–84 DPH hybrids irrespective of genotype, H98 = 98 DPH hybrids irrespective of genotype, Mex = *A. mexicanum* irrespective of sampling time, M112 = 112 DPH *met1*$^{mex/mex}$ hybrids, T112 = 112 DPH *met1*$^{mex/Att}$ hybrids, and Tig = *A. t. tigrinum* irrespective of sampling time.

chromosomal rearrangements, creating a gene order that has not been observed in any other vertebrates. Some of the loci in the *met1* region are associated with bioenergetics and brain development and function. Several of these genes, and many other genes that are not linked to *met1*, are differentially expressed between hybrids with alternate *met1* genotypes. In addition, we showed that many of the genes that were differentially expressed late in the larval period between hybrids with alternate *met1* genotypes were also differentially expressed between *A. mexicanum* and *A. t. tigrinum* at an earlier time of development. These results support the idea that differences between *A. mexicanum* and *A. t. tigrinum* in metamorphic timing and neurodevelopmental gene expression are associated with genetic factors in the *met1* genomic region. Finally, we have shown that despite its profound effects on developmental timing and gene expression, *met1* does not influence the larval growth trajectories of backcrossed hybrids prior to its effects on transcription in the brain. Overall, our study underscores the importance of using an integrative genomics approach to resolve genetic aspects of life history variation.

Supplementary Material

Supplementary tables S1–S5 and figure S1 are available at *Genome Biology and Evolution* online (http://www.gbe.oxfordjournals.org/).

Acknowledgments

This work was supported by the Office of Research Infrastructure Programs at the National Institutes of Health (grant number 2R24OD010435 to S.R.V)., National Science Foundation (grant numbers IBN-9982719, IBN-0242833, IBN-0080112, and DBI-0951484 to S.R.V). R.B.P. was supported by the Wallace Endowment to the Department of Biology at the University of Louisville.

Literature Cited

Bar-Or C, Czosnek H, Koltai H. 2007. Cross-species microarray hybridizations: a developing tool for studying species diversity. Trends Genet. 23:200–207.

Benjamini Y, Hochberg Y. 1995. Controlling the false discovery rate: a practical and powerful approach to multiple testing. J R Stat Soc Ser B Stat Methodol. 57:289–300.

Bolstad BM, et al. 2005. Quality assessment of affymetrix GeneChip data. In: Gentleman R, Carey VJ, Huber W, Irizarry RA, Dudoit S, editors. Bioinformatics and computational biology solutions using R and bioconductor. New York: Springer. p. 33–47.

Bradshaw HD, Schemske DW. 2003. Allele substitution at a flower colour locus produces a pollinator shift in monkeyflowers. Nature 426: 176–178.

Broman KW, Sen WH, Churchill GA. 2003. R/qtl: QTL mapping in experimental crosses. Bioinformatics 19:889–890.

Brown MS, Goldstein JL. 1999. A proteolytic pathway that controls the cholesterol content of membranes, cells, and blood. Proc Natl Acad Sci U S A. 96:11041–11048.

Buchholz DR, Paul BD, Fu L, Shi YB. 2006. Molecular and developmental analyses of thyroid hormone receptor function in *Xenopus laevis*, the African clawed frog. Gen Comp Endocrinol. 145:1–19.

Buckley BA. 2007. Comparative environmental genomics in non-model species: using heterologous hybridization to DNA-based microarrays. J Exp Biol. 209:1602–1606.

Churchill GA, Doerge RW. 1994. Empirical threshold values for quantitative trait mapping. Genetics 138:963–971.

Conesa A, Nueda MJ, Ferrer A, Talon M. 2006. maSigPro: a method to identify significantly differential expression profiles in time-course microarray experiments. Bioinformatics 22:1096–1102.

Crawley MJ. 2007. The R Book. West Sussex (UK): Wiley.

Dennis G, et al. 2003. DAVID: database for annotation, visualization, and integrated discovery. Genome Biol. 4:R60.

Denver RJ, Glennemeier KA, Boorse GC. 2002. Endocrinology of complex life cycles: amphibians. In: Pfaff D, Arnold A, Etgen A, Fahrbach S, Rubin R, editors. Hormones, brains, and behavior. San Diego (CA): Academic Press. p. 469–513.

Feder ME, Mitchell-Olds T. 2003. Evolutionary and ecological functional genomics. Nat Rev Genet. 4:651–657.

Galton VA. 1992. Thyroid hormone receptors and iodothyronine deiodinases in the developing Mexican axolotl, *Ambystoma mexicanum*. Gen Comp Endocrinol. 85:62–70.

Gautier L, Cope L, Bolstad BM, Irizarry RA. 2004. Affy—analysis of Affymetrix GeneChip data at the probe level. Bioinformatics 20: 307–315.

Gould SJ. 1977. Ontogeny and phylogeny. Cambridge (MA): Harvard University Press.

Haley CS, Knott SA. 1992. A simple regression method for mapping quantitative trait loci in line crosses using flanking markers. Heredity 69: 315–324.

Hoekstra HE, Hirschmann RJ, Bundey RA, Insel PA, Crossland JP. 2006. A single amino acid mutation contributes to adaptive beach mouse color pattern. Science 313:101–104.

Hosack DA, Dennis G Jr, Sherman BT, Lane HC, Lempicki RA. 2003. Identifying biological themes within lists of genes with EASE. Genome Biol. 4:R70.

Irizarry RA, et al. 2003. Exploration, normalization, and summaries of high density oligonucleotide array probe level data. Biostatistics 4: 249–264.

Jones CD. 1998. The genetic basis of *Drosophila sechellia*'s resistance to a host plant toxin. Genetics 149:1899–1908.

Joron M, et al. 2006. A conserved supergene locus controls colour pattern diversity in *Heliconius* butterflies. PLoS Biol. 4:e303.

Kosambi D. 1944. The estimation of map distances from recombination values. Ann Eugen. 12:172–175.

Morey S, Reznick D. 2000. A comparative analysis of plasticity in larval development in three species of spadefoot toads. Ecology 81:1736–1749.

Mundy NI. 2007. Coloration and the genetics of adaptation. PLoS Biol. 5: e250.

Newman RA. 1989. Developmental plasticity of *Scaphiopus couchii* tadpoles in an unpredictable environment. Ecology 70:1775–1787.

O'Neill EM, et al. 2013. Parallel tagged amplicon sequencing reveals major lineages and phylogenetic structure in the North American tiger salamander (*Ambystoma tigrinum*) species complex. Mol Ecol. 22: 111–129.

Page RB, Boley MA, Smith JJ, Putta S, Voss SR. 2010. Microarray analysis of a salamander hopeful monster reveals transcriptional signatures of paedomorphic brain development. BMC Evol Biol. 10:199.

Page RB, et al. 2007. Microarray analysis identifies keratin loci as sensitive biomarkers for thyroid hormone disruption in the salamander *Ambystoma mexicanum*. Comp Biochem Physiol C Pharmacol Toxicol. 145: 15–27.

Petranka JW. 1998. Salamanders of the United States and Canada. Washington (DC): Smithsonian Institution Press.

Prahlad KV. 1968. Induced metamorphosis: rectification of a genetic disability by thyroid hormone in the Mexican axolotl *Siredon mexicanum*. Gen Comp Endocrinol. 11:21–30.

Schneider RA, Helms JA. 2003. The cellular and molecular origins of beak morphology. Science 299:565–568.

Semlitsch RD, Wilbur HM. 1989. Artificial selection for paedomorphosis in the salamander *Ambystoma talpoideum*. Evolution 43:105–112.

Shaffer HB, McKnight ML. 1996. The polytypic species revisited: genetic differentiation and molecular phylogenetics of the tiger salamander *Ambystoma tigrinum* (amphibian: caudate) complex. Evolution 50: 417–433.

Shi YB. 2000. Amphibian metamorphosis: from morphology to molecular biology. New York: Wiley-Liss.

Smith JJ, Kump DK, Walker JA, Parichy DM, Voss SR. 2005. A comprehensive expressed sequence tag linkage map for tiger salamanders and the Mexican axolotl: enabling gene mapping and comparative genomics in *Ambystoma*. Genetics 171:1161–1171.

Smith JJ, Voss SR. 2006. Gene order data from a model amphibian: new perspectives on vertebrate genome structure and evolution. BMC Genomics 7:219.

Smith-Gill SJ, Berven KA. 1979. Predicting amphibian metamorphosis. Am Nat. 113:563–585.

Smyth GK. 2004. Linear models and empirical Bayes methods for assessing differential expression in microarray experiments. Stat Appl Genet Mol Biol. 3:3.

Streelman JT, Peichel CL, Parichy DM. 2007. Developmental genetics of adaptation in fishes: the case for novelty. Annu Rev Ecol Evol Syst. 38: 655–681.
Venables WN, Ripley BD. 2010. Modern applied statistics with S. 4th ed. New York: Springer.
Voss SR. 1995. Genetic basis of paedomorphosis in the axolotl, *Ambystoma mexicanum*: a test of the single gene hypothesis. J Hered. 86: 441–447.
Voss SR, Kump DK, Walker JA, Shaffer HB, Voss GJ. 2012. Thyroid hormone responsive QTL and the evolution of paedomorphic salamanders. Heredity 109:293–298.
Voss SR, Prudic KL, Oliver JC, Shaffer HB. 2003. Candidate gene analysis of metamorphic timing in ambystomatid salamanders. Mol Ecol. 12: 1217–1223.
Voss SR, Shaffer HB. 1997. Adaptive evolution via a major gene effect: paedomorphosis in the Mexican axolotl. Proc Natl Acad Sci U S A. 94: 14185–14189.
Voss SR, Shaffer HB. 2000. Evolutionary genetics of metamorphic failure using wild-caught vs. laboratory axolotls (*Ambystoma mexicanum*). Mol Ecol. 9:1401–1407.
Voss SR, Shaffer HB, Taylor J, Safi R, Laudet V. 2000. Candidate gene analysis of thyroid hormone receptors in metamorphosing vs. nonmetamorphosing salamanders. Heredity 85:107–114.
Voss SR, Smith JJ. 2005. Evolution of salamander life cycles: a major-effect quantitative trait locus contributes to discrete and continuous variation for metamorphic timing. Genetics 170:275–281.
Voss SR, et al. 2011. Origin of avian and amphibian chromosomes by fusion, fission, and retention of ancestral chromosomes. Genome Res. 8:1306–1312.
Wilbur HM. 1980. Complex life cycles. Annu Rev Ecol Syst. 11:67–93.
Wilbur HM, Collins JP. 1973. Ecological aspects of amphibian metamorphosis. Science 28:1305–1314.

Associate editor: Patricia Wittkopp